

## **The Chemistry of Fuel Crud Deposits and Its Effect on AOA in PWR Plants**

Jim Henshaw, John C McGuire and Howard E Sims<sup>†</sup>

Ann Tuson, Shirley Dickinson<sup>\*</sup>

Jeff Deshon<sup>+</sup>

<sup>†</sup> BNFL, <sup>\*</sup> AEA Technology, <sup>+</sup> EPRI

### **Abstract**

Models are described for simulating thermal hydraulic and chemical conditions within fuel crud deposits and the transport of Ni/Fe around a PWR circuit. In the crud chemistry model heat transfer takes place by wick boiling in which water flows through the porous deposit and evaporates into steam at the surface of chimneys. The transport and chemistry of dissolved species within the deposit is also modelled. Modelling has also been carried out with a simplified version of this chemistry model coupling the crud thermal hydraulics to the bulk thermal hydraulics. This coupling impacts on the boundary conditions at the crud-water interface and has consequences on the chemistry in the crud. Finally, a brief description of a PWR Ni/Fe release, transport and deposition model is given which has helped explain certain observations in high duty plants undergoing AOA.

### **Introduction**

The axial offset (AO) of a PWR plant is the integrated power output in the top half of the core minus the integrated power over the bottom half, all divided by the total power output. When a PWR is operational this parameter is measured and compared with predictions from a computer code. For most plants these comparisons are good but for a number of years and for some plants operating at high powers, this has not been the case. This AO anomaly (AOA) results from a shift in power output towards the bottom of the core as a result of a fall in the neutron flux in the upper core regions. This has a number of safety implications which could lead to a down-rating of the plant and subsequent economic losses [1].

Axial offset Anomaly (AOA) is caused by the deposition of crud on the fuel pins in the core of a PWR. When significant levels of crud have built up on the pins boron can accumulate in the pores of the crud as a concentrated solution or solid phase and cause the observed flux depression. The mechanism for concentrating boron and the chemistry/thermal hydraulics taking place within the crud have been discussed in reference [2]. The principal cause of AOA is believed by the precipitation of  $\text{LiBO}_2$  at a certain crud thickness, usually a few tens of microns, the exact thickness being determined by the local thermal hydraulics and to a lesser degree the bulk chemistry. In order to avoid AOA a plant needs to avoid achieving this critical crud thickness.

This group has been involved in modelling the phenomenon of AOA and in the following sections a brief review of the various models that have been used and their results are given.

The following section highlights some of the plant observations which the models were developed to explain.

## Plant Observations

Most of these plant observations are based on the work of Byers [1] and are summarised here.

- AOA is first observed in plants where crud deposits are believed to have built up to  $\sim 25 \mu\text{m}$ .
- In some very thick crud deposits ( $>80\mu\text{m}$ ) the boron mineral bonaccordite ( $\text{Ni}_2\text{FeBO}_5$ ) has been identified. This indicates fairly extreme conditions within the crud [3].
- A few plants with thick deposits have seen a layer of  $\text{ZrO}_2$  material some distance above the fuel clad oxide surface, see Figure 1.

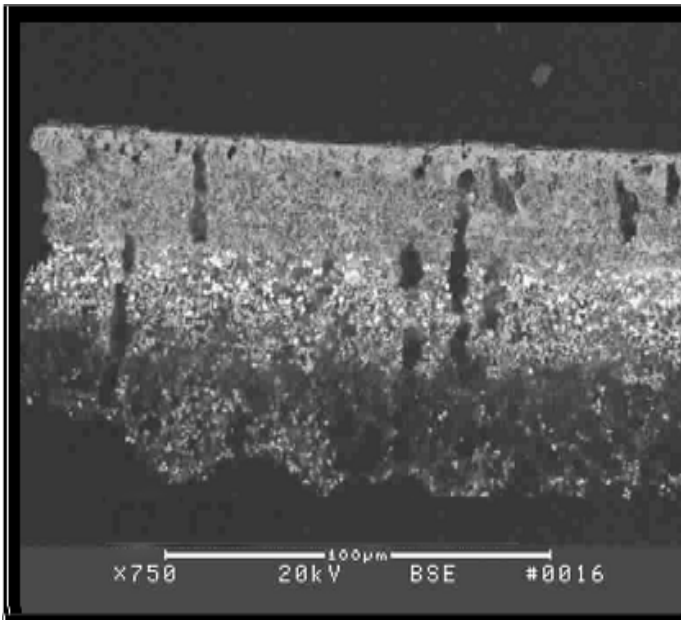


**Figure 1 A thick crud flake showing three distinct layers. The middle white zone contains  $\text{ZrO}_2$ .**

- Examination of fuel crud scrapes indicate a Ni rich deposit compared to crud scrapes from non-AOA plants.
- Thick crud contains relatively less chromium than thin crud.

In the following sections it will be shown how these observations can be explained by the models that have been derived to investigate these phenomena.

## Crud Chemistry Model (CCM)

### *Model Theory*

This section briefly describes a chemistry model of fuel crud deposits in a PWR reactor, which treats the heat transfer, fluid flow and chemical reactions taking place in porous deposits on the fuel pins of the reactor. The model has been described elsewhere [2] so only a brief summary is provided here. The model implements a realistic thermal hydraulics model together with a rigorous treatment of the thermodynamics of the high temperature aqueous solution and includes the following features

- a Wick boiling model;
- radiolysis chemistry of water, taking into account the alpha dose from the  $^{10}\text{B}(n, \alpha)^7\text{Li}$  reaction;
- magnetite dissolution and iron hydrolysis reactions;
- Ni-Fe ferrite dissolution and nickel hydrolysis reactions;
- Ni metal and Ni oxide formation;
- boric acid chemistry and the precipitation of lithium borate;
- non-ideal solution thermodynamics;
- the effect of solute concentration on the saturation temperature and vaporisation enthalpy of water.

The model treats the heat flux, fluid flow and chemical reactions in a deposit unit cell, consisting of one steam chimney and its surrounding porous shell. The model is one dimensional through the depth of the deposit from the bulk solution to the surface of the metal.

### *Thermal Hydraulics, Transport and Chemistry*

The thermal hydraulics model that is used is based on Cohen's one dimensional Wick boiling model [4]. This simulates water transport through the porous deposit and evaporation and steam transport within steam chimneys. The model is derived by considering the heat transfer in the deposit unit cell. Heat transfer is assumed to take place by conduction across the porous shell from the fuel pin towards the bulk coolant and by evaporation of steam at the surface of the chimney, as shown schematically in Figure 2.

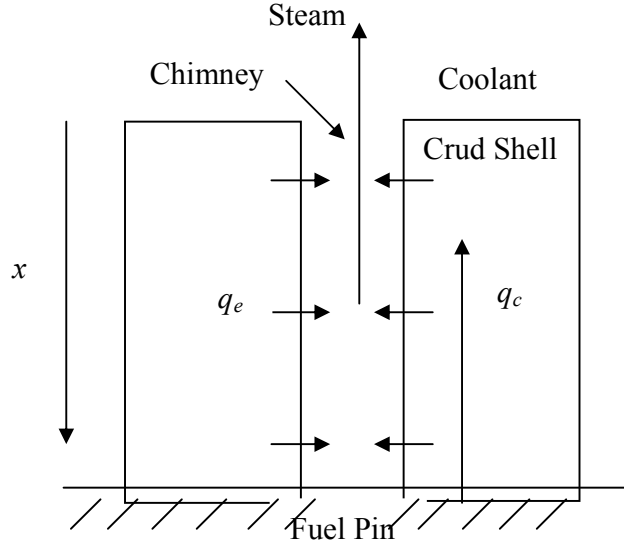


**Figure 2 Schematic diagram of heat transport during wick boiling.  $q_e$  is the evaporative heat flux and  $q_c$  the conductive heat flux.**

By considering heat balance across the cell it can be shown [4] that the temperature distribution is given by

$$\frac{d^2T}{dx^2} - \frac{2\pi r_c N_c h_e}{fk_c} (T - T_s) = 0 \quad (1)$$

Where  $f$  is the fractional area of the porous shell,  $N_c$  is the area density of chimneys,  $r_c$  is the chimney radius,  $k_c$  is the thermal conductivity of the porous shell,  $h_e$  is the evaporative heat transfer coefficient and  $T_s$  is the saturation temperature. This equation is solved subject to the boundary conditions,

$$T = T_{sat} \quad \text{at } x = 0 \quad (2a)$$

$$k_c \left( \frac{\partial T}{\partial x} \right)_{x=d} = \frac{q_0}{f} \quad \text{at } x = d \quad (2b)$$

where  $T_{sat}$  is the saturation coolant temperature,  $q_0$  is the heat flux at the surface of the fuel pin and  $d$  is the thickness of the deposit.

The model used here though differs from the simple Cohen model because terms such as  $h_e$ ,  $T_s$  etc are functions of the thermodynamic activities of water, boric acid and other species within the deposit. These activities are evaluated using non-ideal thermodynamics and by solving the transport and chemical rate equations through the porous material. The flow of liquid into the porous deposit transports dissolved boric acid and lithium hydroxide through the deposit. Also transported are hydrogen and trace amounts of other species arising from the radiolysis of water and the dissolution of metal oxides. These species become concentrated within the porous shell where they react amongst themselves and with the oxides of the deposit. Dissolved species are transported by flow, by diffusion in their concentration gradient and, if they are charged, by drift in the electric potential gradient. For each species in the liquid phase (there is an equivalent equation for the vapour phase species,  $H_2(g)$ ,  $O_2(g)$  and  $H_3BO_3(g)$ ) it is possible to write

$$\frac{\partial C_l}{\partial t} = \left( \frac{\partial C_l}{\partial t} \right)_R + \left( \frac{\partial C_l}{\partial t} \right)_P - \frac{1}{\varepsilon} \frac{\partial J_l}{\partial x} \quad (3)$$

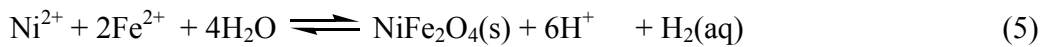
Where  $C_l$  is the concentration in the liquid, and the first term on the right of the equation is due to changing species concentrations by chemical reaction (subscript  $R$  for reaction), the second term is due to liquid/steam partitioning (subscript  $P$  for partitioning) and the third term is due to transport.  $\varepsilon$  is the porosity of the deposit, which is the fraction of free space present per unit volume of crud. These equations are solved for all the species in the deposit and their activities determined while simultaneously solving the Cohen model equations.

The different types of chemical reactions included in the model are summarised below.

(1) The ionisation of water



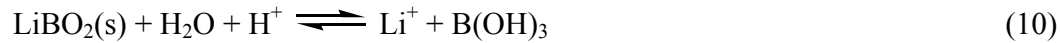
(2) Metal ion hydrolysis reactions



(3) Boric acid equilibria



(4) Precipitation and dissolution reactions



(5) Liquid to vapour partitioning reactions



(6) Radiolysis chemistry of water

All the equations were implemented and solved using the numerical integration program FACSIMILE [5], which uses a form of Gears method for solving stiff differential equations. The following Section discusses some of the results obtained with the model.

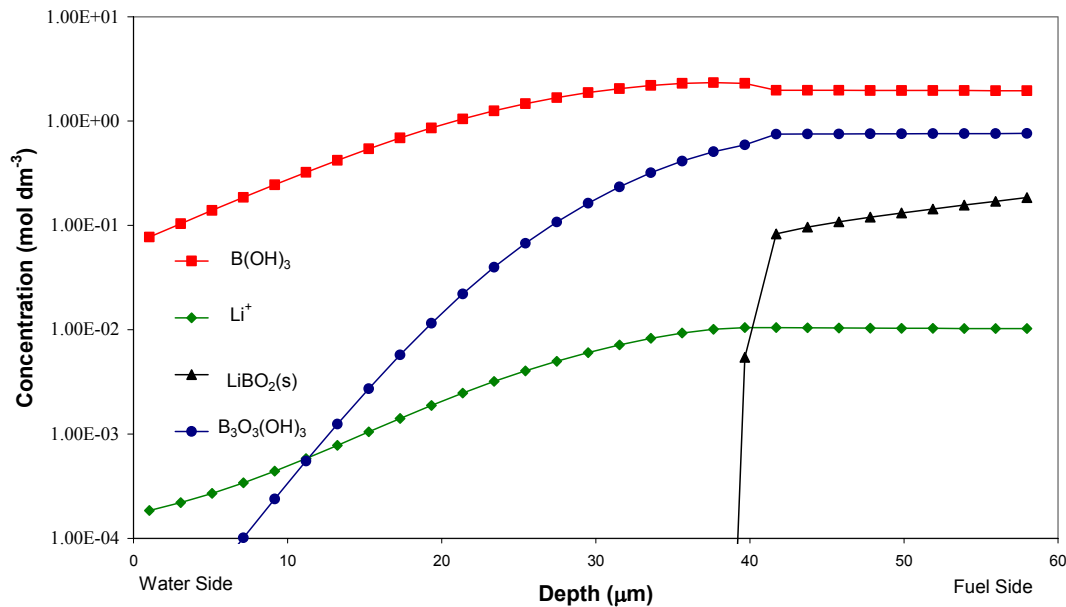
### CCMI Results

Table 1 shows the standard input conditions for which the model was used.

**Table 1 Standard PWR input conditions for the CCM model.**

Parameter	Value
Coolant saturation temperature/ $^{\circ}\text{C}$	345
System pressure/atm	153
Chimney density/ $\text{mm}^2$	3000
Chimney radius/ $\mu\text{m}$	2.5
Porosity	0.8
Tortuosity	2.5
Deposit depth/ $\mu\text{m}$	25-60
Heat flux $\text{W}/\text{m}^2$	$10^6$
Li/ppm	2
B/ppm	1200
$\text{H}_2/\text{cc}$ (STP) $\text{kg}^{-1}$	25
$\gamma$ Dose rate/Mrad $\text{h}^{-1}$	1200
n Dose rate/Mrad $\text{h}^{-1}$	2400
n Flux/ $\text{cm}^{-2} \text{s}^{-1}$	$3.6 \times 10^{14}$

Figure 3 shows how the  $\text{Li}^+$ , Boric acid and  $\text{LiBO}_2(\text{s})$  concentrations vary through a  $59\mu\text{m}$  thick crud deposit for typical PWR conditions.



**Figure 3  $\text{Li}^+$ , Boric acid concentration and amount of  $\text{LiBO}_2(\text{s})$  against depth for a  $59\mu\text{m}$  thick deposit. Calculation with 2ppm Li, 1200ppm B and  $25\text{cm}^3 \text{kg}^{-1}$  (STP)  $\text{H}_2$ .**

The results indicate the boric acid concentration is approximately 2M near the fuel surface (a concentration factor of 25 compared to the bulk). Also important in the liquid phase is the boric acid trimer, which contains approximately 2M boron near the fuel surface. The  $\text{Li}^+$  ion concentration rises to 0.01M (a concentration factor of 54). What is interesting about these results is that  $\text{LiBO}_2(\text{s})$  precipitates at a depth of 35 to  $40\mu\text{m}$ . This is near the crud thickness, based on scrape measurements, where AOA starts to be observed [1]. It should be noted that nothing in the model was adjusted to give this result and it is simply a consequence of the physics and chemistry that have been implemented.

The reason this model predicts precipitation at much smaller crud thicknesses can be understood from Figure 4, which shows how the temperature varies through the crud for a 35 and  $59\mu\text{m}$  thick deposit.

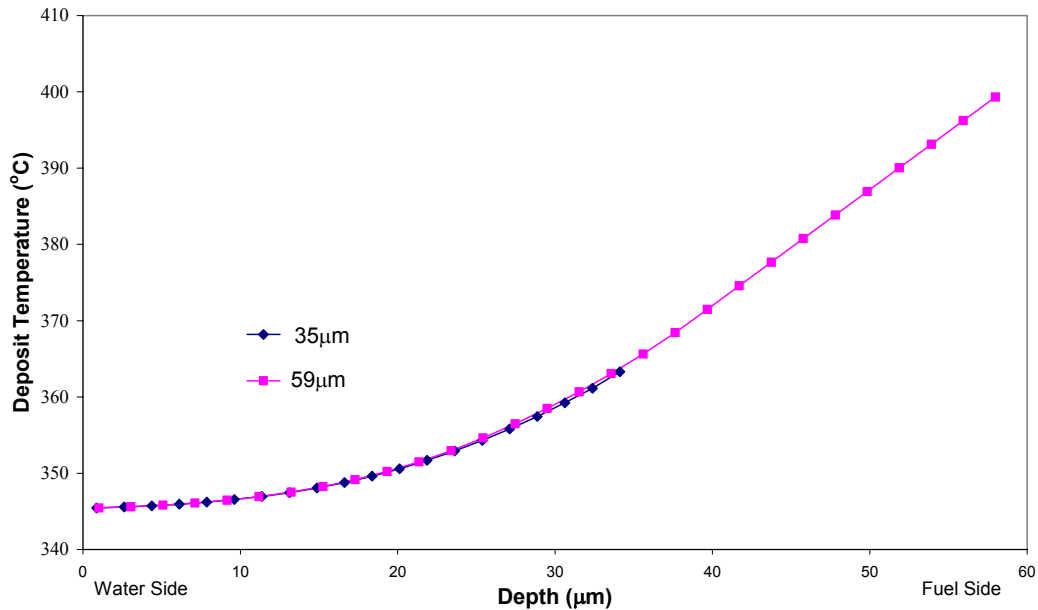


**Figure 4 Temperature across the deposit for a 35 and 59μm thick deposit. Calculation with 2ppm Li, 1200ppm B and 25cm<sup>3</sup> kg<sup>-1</sup> (STP) H<sub>2</sub>.**

Figure 4 indicates the rise in species concentrations towards the bottom of the crud causes a rise in the saturation temperature and because the solubility of LiBO<sub>2</sub>(s) falls with increasing temperature it precipitates. This rise in temperature was not accounted for in previous models.

For the 59μm thick crud the rise in temperature is dramatic, reaching temperatures near 400°C, well above the critical point for pure water (approximately 374°C). Part of the reason for this rise is the fact that as the temperature increases the enthalpy of vaporisation decreases (it is zero at the critical point temperature). This means that less energy is removed by evaporation into the chimney (at the critical point temperature no energy removal occurs by evaporation). The shutting down of evaporation therefore causes the temperature to rise even further. Extreme conditions may therefore exist at the bottom of thick crud and may explain the formation of the mineral bonaccordite [1]. The work of Sawicki indicates temperatures just above 400 °C may be required to form this mineral [3]. The potential effect of reaching near 400 °C on cladding corrosion in the model has not been reconciled yet. It is acknowledged that such temperatures would likely accelerate cladding corrosion and this has not been observed in plants where bonaccordite has been measured or suspected to be present.

Figure 5 shows the variation in pH<sub>T</sub> through the porous deposit for a 35 and 59μm thick deposit.

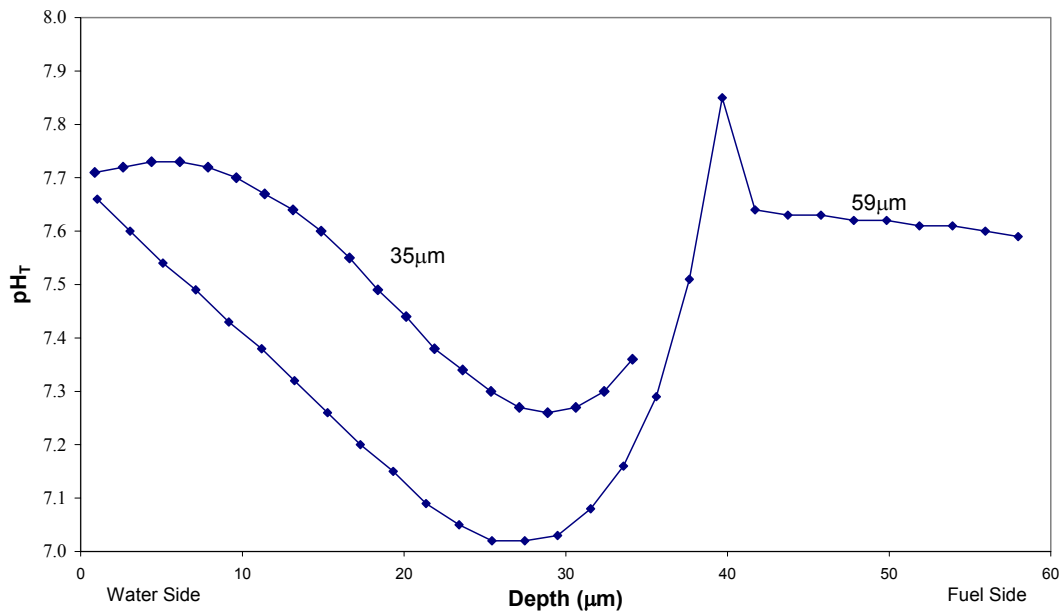


**Figure 5 pH at temperature across the deposit for 35 and 59 μm thick deposits. Calculation with 2ppm Li, 1200ppm B and 25cm<sup>3</sup> kg<sup>-1</sup> (STP) H<sub>2</sub>.**

For the 35 μm thick deposit the pH falls through the deposit from the water side to the fuel side. The pH for the 59 μm thick deposit shows a complicated behaviour with a relatively steady pH near the fuel surface followed by a sudden fall in pH and then rising again towards the water side of the crud. The steady pH near the fuel pin surface is due to the presence of LiBO<sub>2</sub>(s) which buffers the pH in this region. If LiBO<sub>2</sub>(s) was not allowed to precipitate in the model the pH in this region would be very large (9 to 10). For the thick deposit, since ZrO<sub>2</sub> solubility tends to rise with increasing pH, its solubility is likely to be larger nearer the fuel pin surface than at 20 μm away from the surface. The sharp fall in pH away from the fuel pin surface may give rise to ZrO<sub>2</sub> precipitation at this point, providing an explanation for the band of this oxide seen in some thick deposits, but not in thin deposits. The high temperature and high lithium ion concentration near the fuel surface would also facilitate Zr-oxide dissolution in this region.

Figure 6 shows the calculated hydrogen peroxide concentration at the bottom of the deposit as a function of crud thickness for different bulk water boron concentrations.

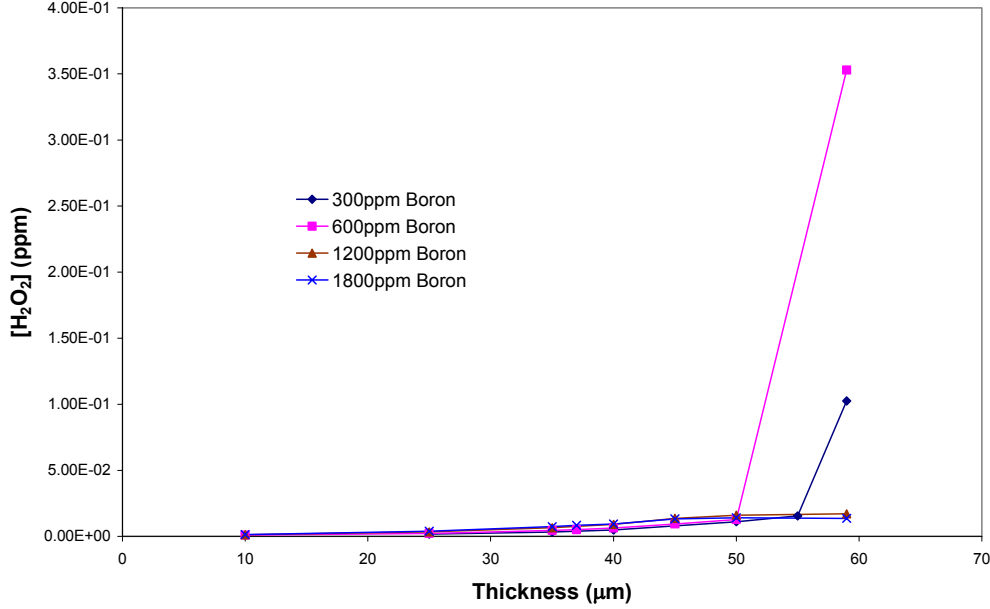


**Figure 6 Hydrogen Peroxide concentrations at the bottom of the crud for different crud thicknesses, at different bulk water boron concentrations.**

It is clear from Figure 6 that the redox conditions could be relatively oxidising at the bottom of thick crud deposits. Peroxide concentrations rise to several hundred ppb, compared to typical bulk water concentrations of less than 1ppb. This is because the chimney through which steam is passing strips hydrogen out of the adjacent water. The process is analogous to a boiling fuel channel in a Boiling Water Reactor but on a micro scale. The observation that thick crud is depleted in chromium supports the existence of oxidising conditions in the crud. This is because chromium solubility increases with increasing oxidising conditions and so is more likely to leach out of thick crud deposits.

### Simplified Chemistry Model

It became clear in using the model described in the previous section that although it explained many of the plant observation it tended to over-estimate the thickness of crud required to observe AOA. In order to account for this CCM was adapted so that the crud thermal hydraulics was coupled to the bulk thermal hydraulics. This coupling is achieved by using the following equation

$$q^{n_q} = q_{fc}^{n_q} + (q_b + q_{nb})^{n_q} \quad (13)$$

Where  $q$  is the total heat flux into the crud,  $q_{fc}$  the heat flux removed by forced convection,  $q_b$  the heat flux due to boiling in the crud and  $q_{nb}$  the heat flux due to nucleate boiling. The Thom-Dittus-Boelter [6] correlation was used to calculate  $q_{fc}$  and  $q_{nb}$  and  $n = 3$  was used in the implementation of the model. This coupling leads to a non-linear equation for the temperature at the crud-water interface that is solved iteratively during the calculation. In simple terms this corresponds to a change in the boundary condition described by equation (2). In addition to coupling the heat transport through the crud with the bulk heat transfer, the mass transfer across the liquid boundary layer was also coupled with the mass transfer through the crud. The solution of this model proved difficult with the full chemistry described above, so this chemistry was simplified by taking out all the reactions with little impact on the Li and B behaviour. Figure 7 is a plot of crud depth required to produce  $\text{LiBO}_2$  precipitation against input power. The calculations discussed in the previous section were all performed at  $1\text{MWm}^{-2}$  and predicted precipitation at 35 to  $40\mu\text{m}$ . Figure 7 shows that at  $1\text{MWm}^{-2}$   $\text{LiBO}_2$  precipitates at between 20 and  $25\mu\text{m}$  more in line with plant observations.

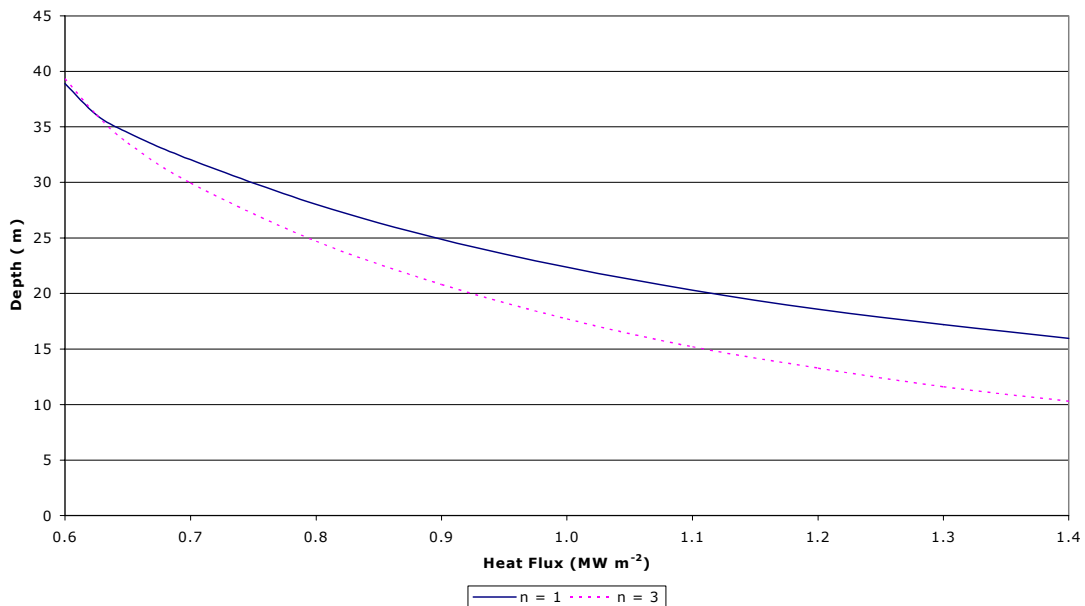


**Figure 7 Plot of depth at which  $\text{LiBO}_2$  precipitates versus Heat Flux**

The main reason for this decrease in crud thickness required to precipitate out  $\text{LiBO}_2(\text{s})$  is because boiling in the crud increases mass transfer of boric acid from the bulk to the crud water interface. This means that the concentration of boric acid at the crud-water interface is significantly larger than in the bulk.

## Ni and Fe PWR Release, Transport and Deposition Model

This section describes a simple model for simulating Ni, Fe release and deposition in a PWR circuit. The model is a simple “box” model in which each compartment (box) represents a particular component of the plant. Within each compartment, the properties of the water and material in the water, are assumed to be the same throughout. The model simulates corrosion release from oxide layers on Stainless Steel and Inconel surfaces; and incorporates solid phase thermodynamics discussed in reference [2].

The particular components of the plant that are modelled are shown in Figure 8, and consist of a cold leg (CL), four core sections, four fuel sections, a hot leg (HL) and two steam generator (SG) sections.

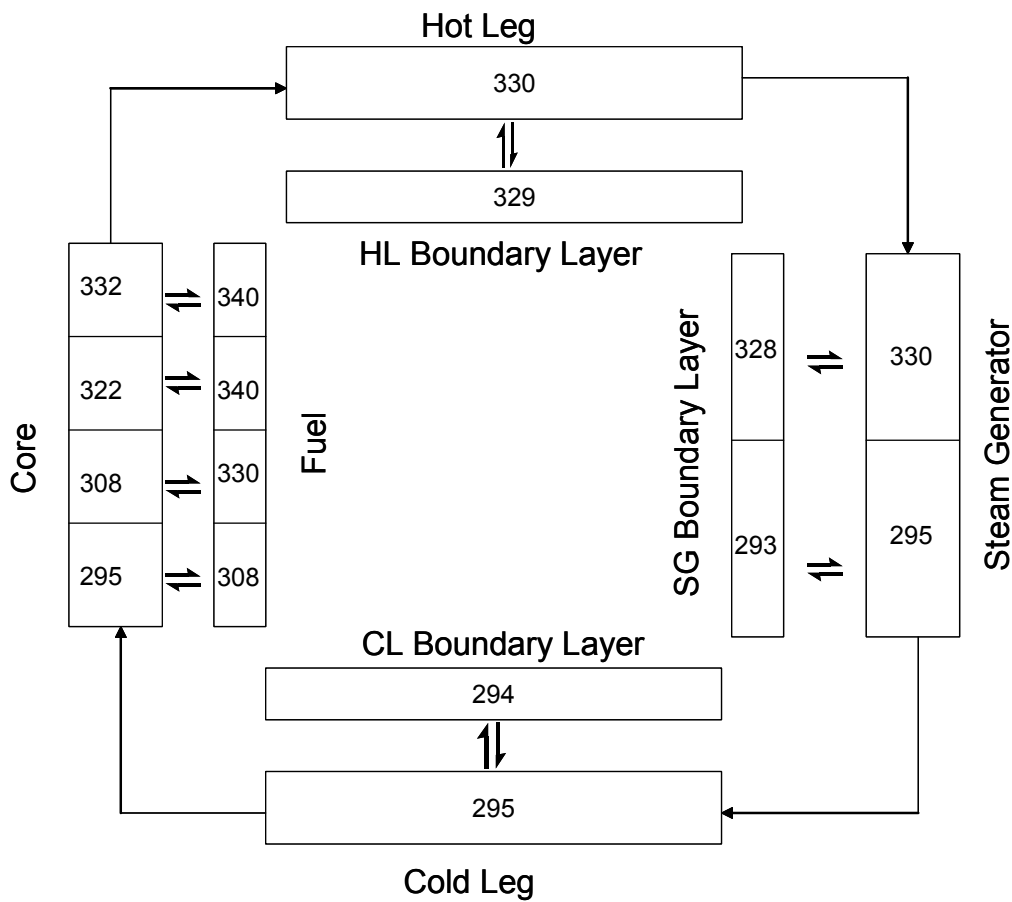


**Figure 8 Schematic diagram of modelled PWR loop. The numbers are the temperatures in degrees C in each section.**

The temperatures for the four fuel sections (referred to as 1,2,3,and 4 starting at the bottom of the core) are typical and were provided by Westacott [7]. The corresponding core sections are simply those parts of the core adjacent to these parts of the fuel, the temperatures in these regions were also provided by Westacott [7]. The temperatures in each of the boxes are shown in Figure 8 and are tabulated in Table 2, along with typical surface areas of each circuit region. Table 2 also shows the other plant and modelling parameters used for the simulations discussed here.

**Table 2 Reactor data input parameters**

Parameter	Value
Areas (m <sup>2</sup> )	380 (CL), 1.16x10 <sup>4</sup> (Fuel), 190 (HL), 3.6x10 <sup>4</sup> (SG)
Flow Rate (m <sup>3</sup> s <sup>-1</sup> )	26
Velocities (ms <sup>-1</sup> )	14.3 (CL), 8.7 (Core), 14.3 (HL), 5.7 (SG)
Temperature (°C)	295 (CL), 295-332 (Core), 308-340 (Fuel), 330 (HL), 330-295 (SG)
Alloy Density (gcm <sup>-3</sup> )	5.2
Oxide Crystal Density (gcm <sup>-3</sup> )	8.4
Porosity	10 <sup>-3</sup>
Tortuosity	2
Stainless Steel Composition	17%Ni, 12%Cr, 71%Fe
Inconel Composition	17%Cr, 10%Fe, 72%Ni

Soluble chemical species are transported around the circuit by flow of the bulk water. The rate of this process is simply determined by the water flow rate in the circuit. Soluble species are also transported between the bulk water and the liquid boundary layer adjacent to the circuit wall by mass transport. In the case of the core soluble species are transported between the bulk water and the fuel pin by mass transport. If precipitation occurs in the boundary layer adjacent to a surface then this is assumed to form the outer oxide layer associated with that surface, or in the case of the fuel this corresponds to deposited crud. The current model does not account for the transport of solid particulate material. In the cold leg (CL), steam generator (SG) and hot leg(HL), release fluxes of Fe(OH)<sub>2</sub> and Ni(OH)<sub>2</sub> species from the surface are included, corresponding to the fluxes of these species generated from corrosion in these regions. These fluxes correspond to transport across the inner oxide layer and they are source terms into the boundary layers adjacent to the particular reactor section. The expressions used for these fluxes are described below.

Bulk fluid transport from one reactor location to an adjacent location is described by

$$\frac{dc_n}{dt} = \left( \frac{dc_n}{dt} \right)_R - k_{flow}(c_n - c_{n-1}) \quad (14)$$

Where  $c$  is a species concentration (a species index is omitted), the index  $n$  labels the particular region of the plant (core, SG, CL, HL),  $n-1$  is the adjacent up-stream section and the first term in this equation  $\left( \frac{dc_n}{dt} \right)_R$  is the rate of change of the species concentration due to chemical reaction.  $k_{flow}$  is simply given by

$$k_{flow} = \frac{Volume \ Flow \ Rate}{V_n} \quad (15)$$

where  $V_n$  is the volume of the region. The transport of species from the boundary layer (or fuel pin) to the bulk water and back is given by equations of the form

$$\frac{dc_j}{dt} = \left( \frac{dc_j}{dt} \right)_R - k_m \frac{S_j}{V_j} (c_j - c_{j-1}) \quad (16)$$

where  $j$  and  $j-1$  label the particular plant region (core, SG, CL, HL) and associated boundary layer,  $k_m$  is the mass transfer coefficient, calculated as described in reference [2], and  $S_j/V_j$  is the surface to volume ratio for the region. For  $Fe(OH)_2$  and  $Ni(OH)_2$  in the CL, HL and SG sections the equations for transport to the boundary layer are, for example,

$$\frac{d[Fe(OH)_2]_{BL}}{dt} = \left( \frac{d[Fe(OH)_2]}{dt} \right)_R - \frac{k_m}{\delta_B} ([Fe(OH)_2]_{BL} - [Fe(OH)_2]_B) + \frac{J_{Fe}^{SS(In)}}{\delta_B} \quad (17)$$

Where  $[Fe(OH)_2]_{BL}$  is the boundary layer concentration of  $Fe(OH)_2$ ,  $[Fe(OH)_2]_B$  its bulk concentration,  $\delta_B$  the boundary layer thickness and  $J_{Fe}^{SS(In)}$  the source flux of  $Fe(OH)_2$  (or  $Ni(OH)_2$ ) from the Stainless Steel or Inconel surface.

In the current model the following soluble species are transported,  $H^+$ ,  $OH^-$ ,  $Fe^{2+}$ ,  $FeOH^+$ ,  $Fe(OH)_2$ ,  $Fe(OH)_3^-$ ,  $Ni^{2+}$ ,  $NiOH^+$ ,  $Ni(OH)_2$ ,  $Ni(OH)_3^-$ ,  $Li^+$ ,  $B(OH)_3$ ,  $B(OH)_4^-$ ,  $B_2O(OH)_5^-$ ,  $B_3O_3(OH)_4^-$ ,  $B_3O_3(OH)_3$ . There are therefore 16 species and 16 boxes, resulting in 384 ordinary differential transport equations to be solved. In addition to these equations the chemical rate equations in each box are also solved and these are described briefly in the following section.

The release flux  $J_{Fe}^{SS(In)}$  is calculated using a similar approach to Cooke et al[8] with the assumptions that

1. The inner oxide of Stainless Steel is  $FeCr_2O_2$  and  $NiFe_2O_4$ , and for Inconel it is Ni and  $FeCr_2O_4$ .
2. The volume of the inner oxide is equal to the volume of alloy that has corroded.
3. Chromium is retained in the inner oxide layer.
4. There are no concentration gradients within the metal alloy.
5. Corrosion occurs by parabolic kinetics.

These assumptions lead to the following equations for the release of Fe from stainless steel with similar equations for Inconel release.

$$J_{Fe}^{ss} = \frac{a_3^{ss} \dot{m}}{A} \quad (18)$$

where

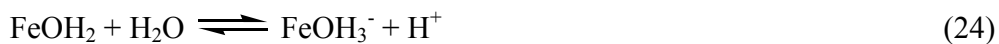
$$a_3^{ss} = \frac{x_{Fe}}{MW_{Fe}} - \frac{a_1^{ss}}{MW_{FeCr_2O_4}} - 2a_2^{ss} \quad (19)$$

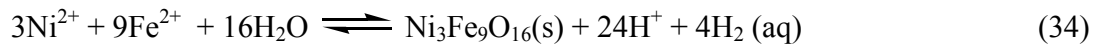
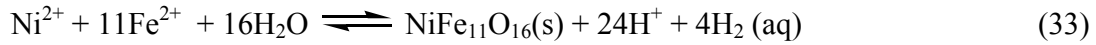
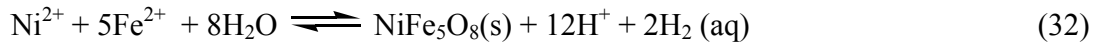
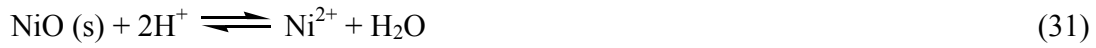
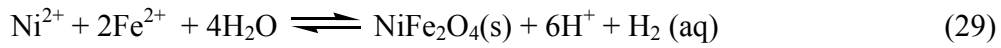
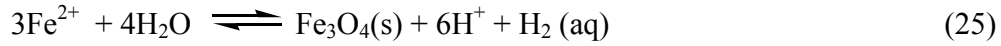
$$a_1^{ss} = \frac{1}{2} \frac{MW_{FeCr_2O_4}}{MW_{Cr}} x_{Cr} \quad (20)$$

$$a_2^{ss} = \frac{\rho_{oxide}}{MW_{NiFe_2O_4}} \left( \frac{1}{\rho_{alloy}} - \frac{a_1^{ss}}{\rho_{oxide}} \right) \quad (21)$$

( $A$  is the area of the plant section,  $x$  is the fraction of the metal in the alloy,  $MW$  refer to molecular weights and the oxide density is  $(1-\phi_i)$  times the crystal density). The rate of corrosion,  $\dot{m}$ , was obtained from an empirical fit to laboratory corrosion data.

In each of the 16 boxes the following chemistry is considered





along with the boric acid equilibria.

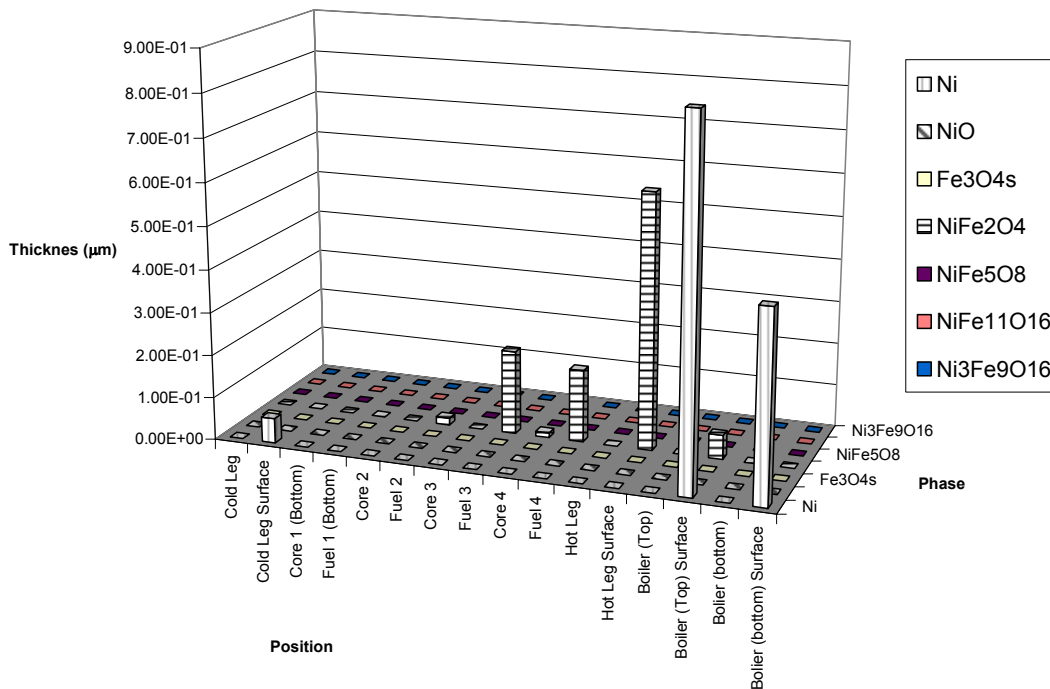


Table 3 is a comparison of the model with plant data, nothing in the model was adjusted to obtain this agreement.

**Table 3 Comparison of circuit transport model with plant data**

	Model Prediction	Polley/Pick [9 ]Plant Analysis
Total oxide on Inconel (kg)	21.5	12.4 – 25
Total oxide on Stainless Steel (kg)	0.6kg	2.4-11.2
Ni Release Rate ( $\text{g m}^{-2} \text{y}^{-1}$ )	0.14	0.55
Fe Release Rate ( $\text{g m}^{-2} \text{y}^{-1}$ )	2.03	5.7
Soluble Fe (ppb)	1.6-1.9	0.8 – 2.7
Soluble Ni (ppb)	0.03	0.03 – 0.4

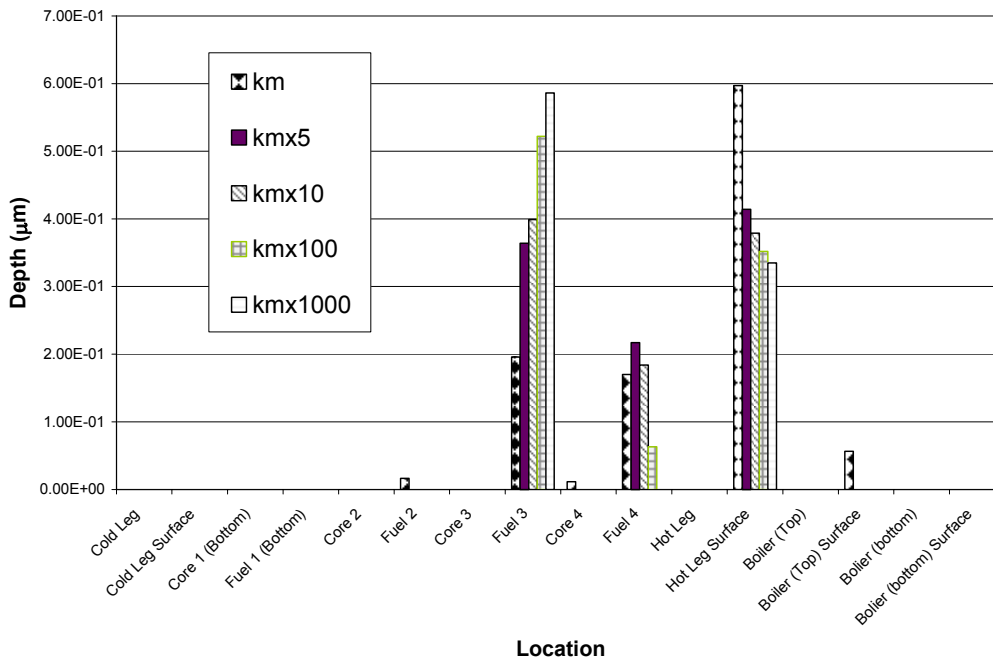
Figure 9 shows the predictions of the model under standard operating (3ppm Li, 1200ppm B and 30 cc/kg H<sub>2</sub>) conditions after a three 12 month cycles of the plant..



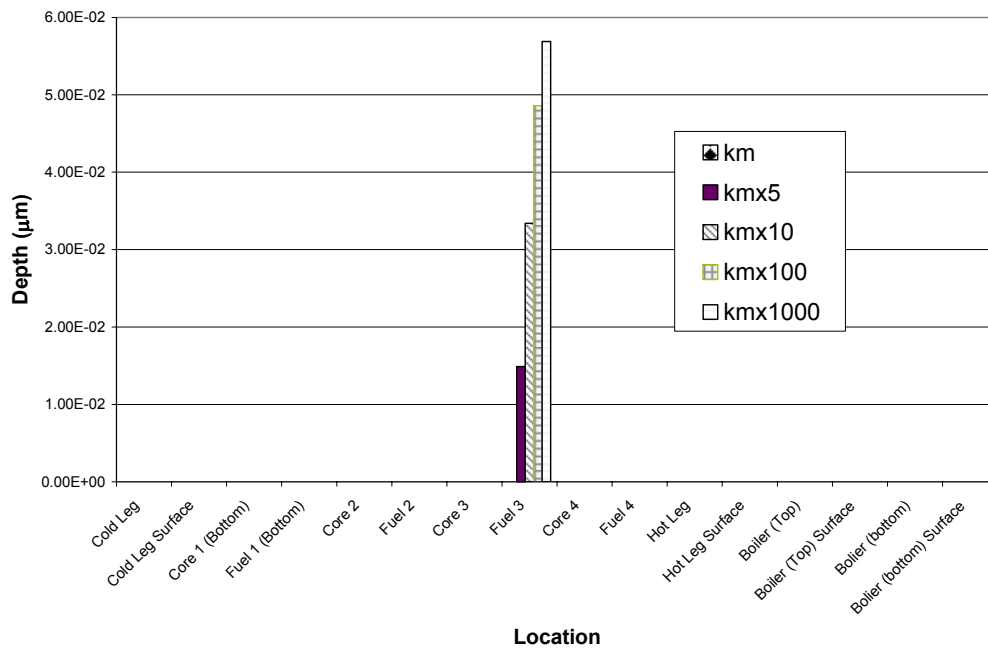
**Figure 9 Plot of Ni and Fe phases present at various locations in the plant circuit.**

Figure 9 shows that most of the Ni entering the circuit exists as Ni metal on the steam generator surfaces, while Fe exists as Ni-ferrite either on the fuel in the top of the core, in the hot leg and on the steam generator.

Figures 10 and 11 shows what happens when the mass transport rate  $k_m$  in the top half of the core is increased.



**Figure 10** Plot of amount of Ni-ferrite depth at all locations in the plant for different mass transfer rates in the core.



**Figure 11** Plot of amount of NiO depth at all locations in the plant for different mass transfer rates in the core.

Both Ni and NiFe<sub>2</sub>O<sub>4</sub> are removed from the steam generator, however there is over ten times more Ni metal on the SG surface so once all the ferrite is removed from the steam generator this part of the plant primarily releases Ni. This Ni released from the steam generator is deposited as NiO, the most stable phase, on the fuel pins. This is why high duty cores have a higher NiO content.

## Summary

The various models for the chemistry/thermal hydraulics in PWR fuel crud and the model for release and transport of Ni and Fe in a PWR circuit help offer explanations for several observations made on high duty cores suffering from AOA.

- The fact that AOA occurs at crud thickness of 20µm is due to the precipitation of LiBO<sub>2</sub>. This precipitates out because of the increased saturation temperature in the crud. The saturation temperature rises because boric acid concentrates in the water.
- Bonaccordite forms because temperatures within thick crud (>80 µm) can approach 380 – 400°C, providing the extreme conditions necessary for its formation.
- ZrO<sub>2</sub> precipitates out at about 10 to 20µm from the crud-pin surface because of a sharp pH fall that occurs in this region. This occurs because the precipitation of LiBO<sub>2</sub> buffers the pH.
- Thick crud is depleted in Cr because oxidising conditions can exist in such crud. Such conditions arise because H<sub>2</sub> is stripped out of the water within the crud in steam chimney's and radiolysis takes place.
- AOA crud is rich in NiO because large deposition rates in the core due to boiling cause the Ni-ferrite in the steam generator to be removed and the plant is operating in a regime where only Ni is released from the steam generator. This released Ni deposits as NiO the stable phase on the fuel pins.

Further work is being undertaken to refine the current models.

## Acknowledgements

This work was funded by the UK's Health and Safety Executive, British Energy and EPRI. Thanks also go to Keith Garbett (Consultant to British Energy) and Art Byers, Dave Chapman (Westinghouse).

## References

---

- 1 (a) P Frattini, E Blandford, D Hussey, A Morvan, J Blok, E Decossin and N Faner, Modelling Axial Offset Anomaly, paper 7.1, Proceedings of the International Conference on Water Chemistry of Nuclear Reactor Systems, San Francisco, October 2004. (b) A Byers and J Deshon, Structure and Chemistry of PWR CRUD, paper 7.5, Proceedings of the International Conference on Water Chemistry of Nuclear Reactor Systems, San Francisco, October 2004.
- 2 (a) J Henshaw, J C McGuire, S Dickinson, H E Sims and A Tuson, Modelling PWR Fuel Corrosion Product Deposition and Growth Process, Interim Report EPRI, Palo Alto, 2004, 1009734, (b) J. Nuc. Mat., 353, 1, (2006). (c) S Dickinson, J Henshaw, J C McGuire and H E Sims, "Modelling PWR Corrosion Product Deposition and Growth Process", EPRI 1011743, 2005.
- 3 J A Sawicki, Nuclear Chemistry Model of Borated Fuel Crud, Proceedings of the International Conference on Water Chemistry of Nuclear Reactor Systems, Avignon, April 2002.
- 4 P Cohen, Heat and Mass Transfer for Boiling in Porous Deposits with Chimneys, AIChE Symposium Series, Vol. 70, No. 138, pp. 71-80, 1974.
- 5 FACSIMILE, a numerical integration package, sold by MCPA Software Ltd, [www-mcpa-software.com](http://www-mcpa-software.com).
- 6 J R S Thom, W M Walker, T A Fallon and G F S Reisling, Boiling in Subcooled Water During Flow up Heated Tubes or Annuli, Symposium on Boiling Heat Transfer, IMechE (London), 1965.
- 7 J Westacott, private communication.
- 8 W G Cook, D H Lister and J M McInerney, Water Chemistry in Nuclear Reactor Systems 8. p 59, BNES (2000).
- 9 M V Polley and M E Pick, Iron, nickel and chromium mass balance in Westinghouse PWR primary circuits, p 63, Water Chemistry in Nuclear Reactor Systems 4. BNES (1986).